AIAA-2000-1459

PREBUCKLING AND POSTBUCKLING RESPONSE OF TAILORED COMPOSITE STIFFENED PANELS WITH AXIAL-SHEAR COUPLING

Richard D. Young*
NASA Langley Research Center
Hampton, Virginia 23681-2199

Michael W. Hyer†
Virginia Polytechnic Institute and State University
Blacksburg, Virginia 24061

and

James H. Starnes, Jr.‡
NASA Langley Research Center
Hampton, Virginia 23681-2199

Abstract

Results of a numerical parametric study of the prebuckling and postbuckling response of tailored composite stiffened panels with axial-shear coupling are presented. In the stiffened panels, axial-shear stiffness coupling is created by rotating the stiffener orientation and tailoring the skin laminate anisotropy. The panels are loaded in axial compression and the effects of stiffener orientation and skin anisotropy on the panel stiffness, buckling parameters, and axial-shear coupling response are described. Results are obtained from a nonlinear general shell finite element analysis computer code. The prebuckling and postbuckling responses can be affected by both the stiffener orientation and skin laminate anisotropy, and the effects are different and load dependent. The results help identify different mechanisms for axial-shear coupling, and show that a load-dependent structural response can be controlled by selecting appropriate stiffener and skin parameters.

Introduction

Stiffened laminated composite panels are increasingly being used in structural applications. Stiffened panels are typically utilized because of their structural efficiency and their ability to support additional load after the skin has buckled. The use of laminated fiber-reinforced composites has increased due to their high strength-to-weight and stiffness-to-weight ratios, and the ability to tailor laminate properties for specific applications.

Since experimental studies have shown that composite stiffened panels can exhibit substantial postbuckling strength (e.g., Refs. 1 and 2), some design practices allow the skin of certain stiffened components to buckle at load levels below design ultimate load conditions. Starnes, et al.[1] presented the results of an experimental and numerical study of postbuckled compression-loaded panels with four I-shaped longitudinal stiffeners. In the experiments some panels supported as much as three times their initial buckling loads before failing.

In some aerospace applications, stiffened panels have been structurally tailored by introducing axial-shear stiffness coupling to control aeroelastic deformations and to improve structural performance (e.g., Refs. 3 and 4). Two techniques have been applied for structural tailoring of stiffened panels. Axial-shear stiffness coupling has been incorporated in metallic stiffened panels by utilizing skewed stiffeners, i.e., stiffeners not aligned with the primary loading direction. In stiffened panels with laminated composite skins, axial-shear stiffness coupling has been generated by rotating the principal direction of orthotropy of the laminated skin relative to the principal loading direction. Historically, efforts to create axial-shear stiffness coupling through structural tailoring have considered only the prebuckling response of the panels. A recent experimental and numerical study[5] conducted by the present authors has reported on the effects of tailoring both skin laminate anisotropy and stiffener orientation on the prebuckling and postbuckling response of stiffened composite panels subjected to an end shortening displacement. The current paper is an extension of the study initially reported in Ref. 5.

The present paper presents the results of a numerical parametric study that was conducted to examine in depth the potential for tailoring the prebuckling and postbuckling response of composite stiffened panels with axial-

* Aerospace Engineer, Mechanics and Durability Branch. Member, AIAA.
† Professor, Department of Engineering Science and Mechanics. Associate Fellow, AIAA; Fellow, ASME; Vice President, ASC.
‡ Chief Engineer, Structures and Materials Competency. Fellow, AIAA.

shear coupling. The conclusions from Ref. 5 indicate that the mechanisms that control the axial-shear coupling response of the stiffened panels are the stiffener properties (orientation and stiffness), and the skin anisotropy (membrane stiffness coupling, and bending stiffness coupling). Configurations are considered herein which either address each of these mechanisms independently, or address combinations of the different mechanisms to tailor the axial-shear coupling response in the prebuckling and postbuckling load ranges. The geometry of the stiffened panels analyzed in the present parametric study is the same as the panels that were tested in Ref. 5. The anisotropy of the skin of the test specimens was varied by rotating a single skin laminate by an angle β equal to -20°, 0°, or 20° relative to the axial direction. For the present parametric study, skin anisotropy is specified by selecting skin laminates that exhibit specific types of anisotropic stiffness coupling. The numerical models that were verified by comparing the measured and predicted responses in Ref. 5 are used to analyze these additional panel configurations. Nonlinear postbuckling analyses are conducted for applied end shortening up to four times the end shortening associated with linear buckling of each configuration. For each configuration that is considered, the prebuckling stiffness, the linear buckling parameters, the postbuckled deformation shape, and the prebuckling and postbuckling force-coupling response are described. The results in Refs. 5 and 6, and the present paper represent part of a more extensive study that was documented in detail in Ref. 7.

Test Specimens and Summary of Results from Ref. 5

In the experimental and numerical study described in Ref. 5, the structural configuration studied consisted of a rectangular graphite-epoxy laminated panel with a single centrally-located I-shaped graphite-epoxy stiffener. Axial-shear stiffness coupling was introduced by rotating the orientation of the stiffener, the principal direction of orthotropy of the skin, or both. The structural parameters varied in the study are shown in Fig. 1. The stiffener orientation is represented by the angle α, and the orientation of the principal direction of orthotropy of the skin laminate is represented by the angle β. A uniform end-shortening displacement u is applied to the upper end of the panel in the axial, or x, direction, and the axial displacement of the lower end is restrained. The upper and lower ends are clamped and the lateral displacement associated with shear, represented by v, is constrained. The unloaded sides are simply supported. The axial compressive force corresponding to the applied end-shortening is represented by P_x, and the shear force reaction generated by the axial-shear stiffness coupling is represented by P_{xy}. The amount of axial-shear stiffness coupling in the panel

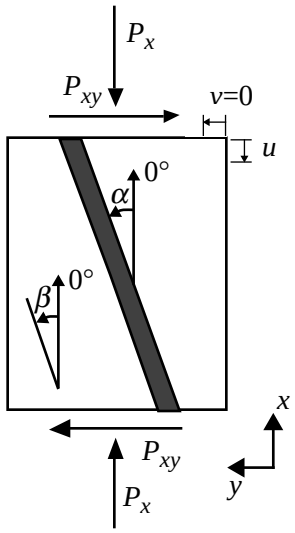

Fig. 1 Structural parameters studied.

is represented by the force coupling ratio, P_{xy} / P_x. The panel test results reported in Ref. 5 are for panels that were fabricated from Hercules Inc. AS4-3502 graphite-epoxy unidirectional preimpregnated tape. Nominal lamina elastic properties for this graphite-epoxy system are given in Table 1. All components were constructed from 16-ply laminates. The nominal stacking sequence for the skin laminate was $[\pm 45 / \mp 45 / 0_3 / 90]_s$. Each test panel had this stacking sequence, with the entire laminate rotated an angle β equal to -20°, 0°, or 20° relative to the axial direction. The stiffener was an I-stiffener with all sections made with a $[\pm 45/0/90]_{2s}$ laminate. Photographs of a typical test panel and stiffener cross-section are shown in Fig. 2. The test specimens have a length of 24.0 inches and a width of 16.5 inches. On each end of the panel, 1.5 inches of the length of the panel is encased in a potting material. On the unloaded sides, knife-edge supports are applied 0.25 inches from the edge of the panel. Five panels were fabricated and tested. The stiffener and skin configurations for these panels

Table 1 Typical material properties: Hercules AS4-3502 graphite-epoxy tape

E_1	20.9 Msi
E_2	1.578 Msi
G_{12}	0.886 Msi
ν_{12}	0.297
V_f	0.660
t_{ply}	0.00490 in.

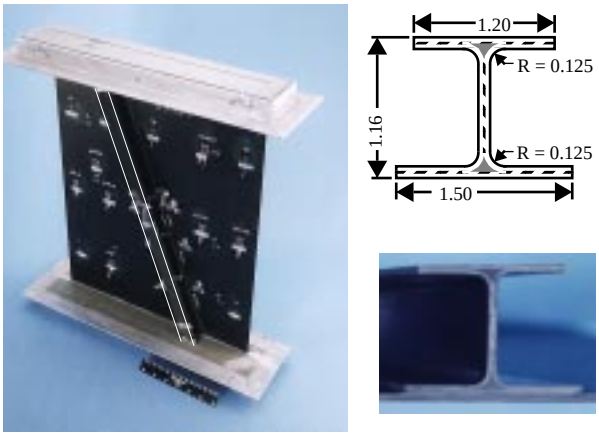

Fig. 2 Typical test panel for experiments reported in Ref. 5.

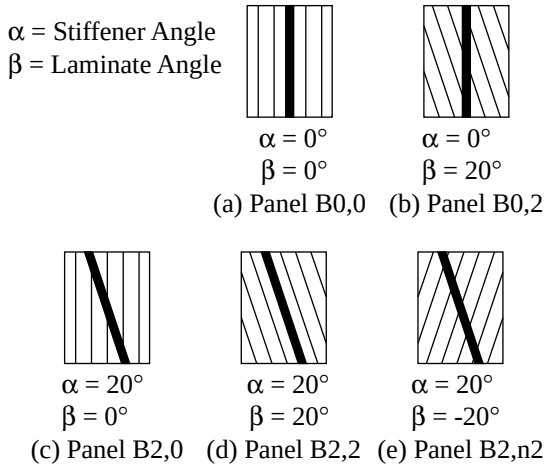

Fig. 3 Test panel configurations studied in Ref. 5. For the panel identification convention (B*x*,*y*), *x* represents the angle α and *y* represents the angle β, where 0, 2, and n2 indicate 0°, 20° and -20°, respectively.

are shown in Fig. 3. Each configuration is represented by a schematic which indicates the stiffener and skin orientations. In Ref. 5, buckling parameters, prebuckling and postbuckling stiffnesses, and force-coupling versus end-shortening results from the experiments are compared to predicted responses obtained from nonlinear finite element analyses conducted using the STAGS (STructural Analysis of General Shells) structural analysis code.[8] It was observed that the axial-shear coupling response of the panels was significantly altered by rotating the stiffener and/or rotating the principal direction of orthotropy of the skin, and that the response was load dependent.

The measured and predicted force-coupling results that were shown in Ref. 5 for the five panels that were tested have been reproduced in Fig. 4. In Fig. 4, the end displacement u is normalized by the end displacement u^o_{cr}, associated with linear buckling of the configuration with the stiffener and skin unrotated, i.e., panel B0,0. The predicted force-coupling results in Fig. 4 support the following observations:

- The force-coupling response of the configuration with the stiffener and skin unrotated is approximately zero for all load ranges.
- The configuration with the unrotated stiffener and the skin rotated exhibits axial-shear stiffness coupling due to skin anisotropy. The amount of force coupling is constant in the prebuckling load range, and decreases in the postbuckling load range (i.e., decreases from 2.54% to 1.69%).
- The configuration with the stiffener rotated and the unrotated skin exhibits axial-shear stiffness coupling due to the skewed stiffener. The amount of force coupling is constant in prebuckling, and increases in the postbuckling load range (i.e., increases from 4.97% to 12.15%).

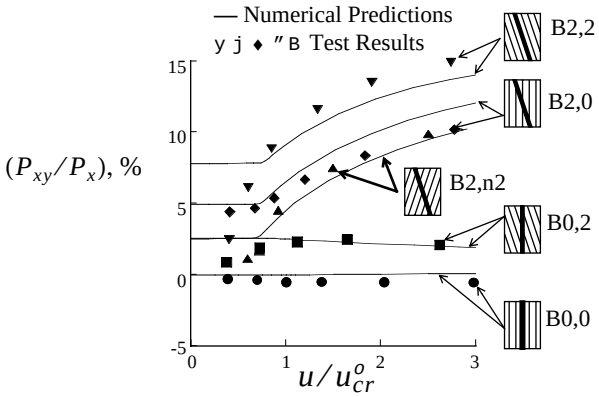

Fig. 4 Predicted and measured force-coupling response for experiments reported previously in Ref. 5.

- The force-coupling response is increased if the skin is rotated in the same direction as the stiffener rotation (the range of the response is 7.84% to 14.17%, compared to 4.97% to 12.15% for the case with the stiffener rotated and the unrotated skin). Rotating the skin in the opposite direction of the stiffener rotation decreases the force-coupling response (the range of the response is 2.57% to 10.24%).

In addition, good correlation between the experimental and predicted panel stiffnesses and buckling parameters reported in Ref. 5 verified the accuracy of the finite element models and indicated that similar finite element models could be used with confidence to predict the response of additional panel configurations that were not tested.

Numerical Model

Finite element models were developed for each panel configuration and analyzed with the STAGS (STructural Analysis of General Shells) structural analysis code.[8] The finite element models were developed to be consistent with the details of the test specimens. A typical model is shown in Fig. 5 and has 4364 active degrees of freedom. The panel's full length (including the length of the sections that would be potted for a test) was modeled. To predict accurately the postbuckling behavior of the panels, each section of the stiffener cross-section was modeled using plate elements.[6] The attachment flanges of the stiffener were modeled as eccentric plate elements joined to the skin elements. The plate element used was the STAGS 410 displacement-based four-node quadrilateral shell element[9] with three translational and three rotational degrees of freedom per node. The thicker lines around the edges of the model in Fig. 5 indicate lines along which the displacement normal to the panel surface was constrained to reflect the support that would be provided by the potting and the knife-edge supports for a test specimen. The bottom edge of the model was fully constrained. The model was loaded by specifying a uniform u displacement on the top edge. The net axial and shear loads, P_x and P_{xy}, were determined by summing the reactions. Linear bifurcation buckling analyses were conducted to determine the effect of structural tailoring and boundary conditions on the linear prebuckling response and the buckling response. Nonlinear postbuckling analyses were conducted to determine how the responses changed in the postbuckling load range. Eigenvectors from the linear bifurcation buckling analyses were used to prescribe initial geometric imperfections that provide a smooth transition from prebuckling to stable postbuckling equilibrium.

Stiffener and Panel Properties

The composite panels considered herein are constructed from the same graphite-epoxy material that was used for the test specimens in Ref. 5. The composite stiffeners, which were shown in Fig. 2, are constructed from $[\pm 45/0/90]_{2s}$ laminates and have 0° graphite-epoxy material filling the triangular-shaped voids at the top and bottom of the stiffener web. To examine independently the effect of the stiffener orientation and stiffness on the axial-shear coupling response of the stiffened panels, panel configurations are also considered which are constructed entirely from 2024 aluminum alloy (E = 10.5 Msi, ν = 0.33). The isotropic material is selected to eliminate any suspicions that the computed responses for these panels are related in any way to material anisotropy. The first configurations that are considered are sized to have the same axial stiffness as panel B0,0. To match

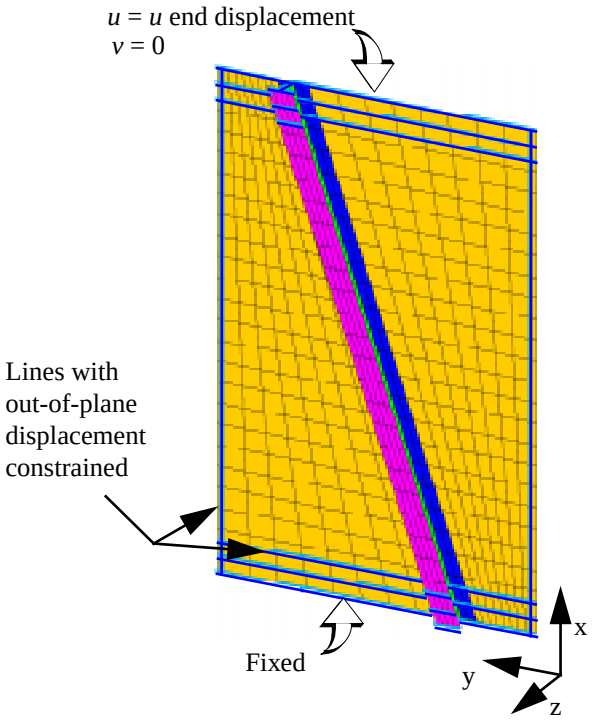

Fig. 5 Typical finite element model.

the axial stiffness, i.e., the *EA*, of the $[\pm 45/\mp 45/0_3/90]_s$ graphite-epoxy laminate, the aluminum skin thickness is set to 0.0771 in. The axial stiffness of the graphite-epoxy stiffener is matched by an aluminum stiffener with the same stiffener dimensions as shown in Fig. 2 and component thicknesses equal to 0.0678 in.

Numerical Results

Effect of Stiffener Orientation

Three all-aluminum panel configurations are analyzed that utilize the skin and stiffener dimensions previously described. The panels, identified as Al-B0, Al-B1, and Al-B2, designate all-aluminum panel configurations with the stiffener rotated 0°, 10°, and 20°, respectively. The prebuckling stiffnesses for these panels are 16,630; 16,530; and 16,270 kips, respectively. The reduction in axial stiffness that occurs when the stiffener is rotated reflects the fact that the stiffener axis is not aligned with the principle loading direction. The linear buckling loads of the three panels are 8.25, 7.70, and 6.48 kips, respectively. Thus, rotating the stiffener by 10° and 20° causes reductions in the buckling load of 7% and 21%, respectively, relative to the panel with the unrotated stiffener. The reduction in buckling load that occurs when the stiffener is rotated is partially associated with the re-

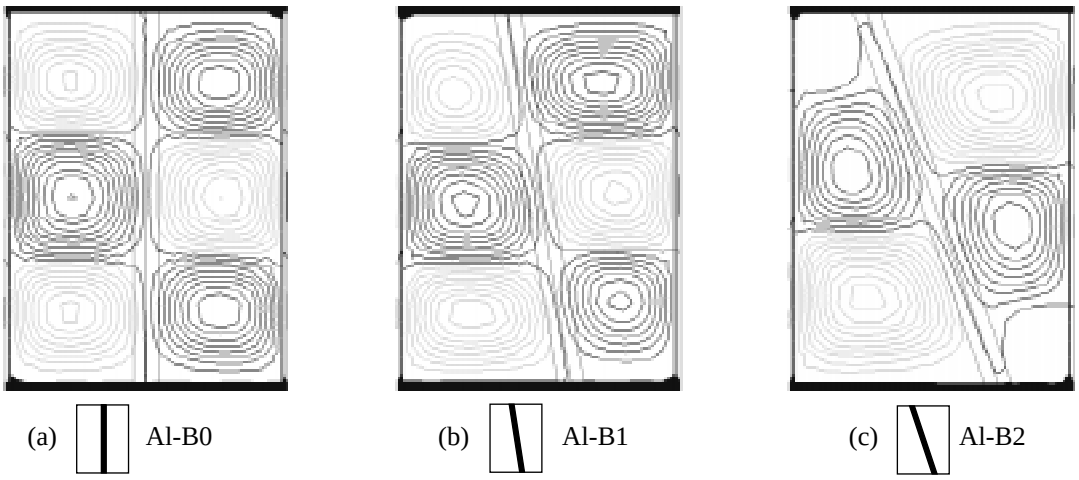

Fig. 6 Postbuckling shapes of all-aluminum panels with the stiffener rotated 0°, 10°, and 20°.

duction in the load supported in the stiffener, but is mostly due to the increase in the width of the skin sections that is introduced when the stiffener is rotated. Contour plots of the out-of-plane displacement in the skin at $u/u_{cr}^{lin} = 4$ are shown in Fig. 6. The contour plots in Fig. 6 indicate that for the all-aluminum panels, the postbuckling deformations have three axial half-waves when the stiffener is unrotated and rotated 10°, and two axial half-waves when the stiffener is rotated 20°. The force-coupling versus end-shortening responses for these panels are shown in Fig. 7. The force coupling for panel Al-B0 is zero, as expected. When the stiffener is rotated 10°, the force-coupling response (i.e., P_{xy}/P_x) is 2.63% in the prebuckling load range, and increases to 7.33% in the postbuckling load range. The force-coupling response of panel Al-B2 varies from 4.95% to 11.77% and is very similar to the response for panel B2,0 (where the force coupling increased from 4.97% to 12.15%).

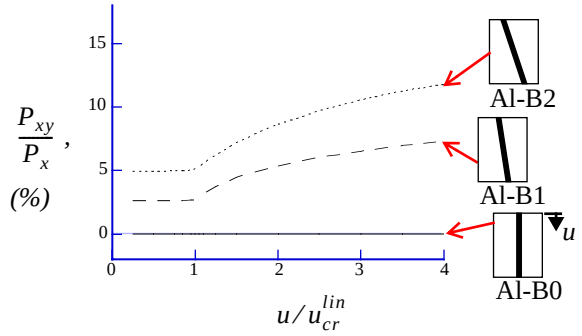

Fig. 7 Force-coupling response of all-aluminum panels with stiffener rotated 0°, 10°, and 20°.

Effect of Stiffness of Stiffener

The effect of the stiffness of the stiffener on the axial-shear coupling response of the panels with skewed stiffeners is examined by considering all-aluminum panels with the thickness of the stiffener components doubled to 0.1356 in., while keeping the skin thickness equal to 0.0771 in. The panels, identified as Al-C1 and Al-C2, designate all-aluminum panel configurations with the more-rigid stiffener rotated 10°, and 20°, respectively. The prebuckling stiffnesses for panels Al-C1 and Al-C2 are 19,430; and 18,820 kips, respectively. The linear buckling loads of the panels are 9.88, and 8.15 kips, respectively. Contour plots of the out-of-plane displacement in the skin at $u/u_{cr}^{lin} = 4$ are shown in Fig. 8. The contour plots in Fig. 8 show that the panels with more-rigid stiffeners have postbuckling deformations with a higher number of half-waves in the axial direction, and smaller out-of-plane deformations in the skin-stiffener attachment region. The change in the deformation shape could strongly influence failure by skin-stiffener separation. The force-coupling versus end-shortening responses for panels Al-B1, Al-B2, Al-C1, and Al-C2 are compared in Fig. 9. The more-rigid stiffener causes the force-coupling response to be higher, compared to the response for the original stiffener, over the entire range of loading. The force-coupling response increases from 4.71% to 8.57% for panel Al-C1, and from 8.90% to 17.00% for panel Al-C2.

Variations in Force-coupling Response in the Postbuckling Load Range for Panels with a Rotated Stiffener

The force-coupling responses of the all-aluminum panels with a rotated stiffener all demonstrate the same general behavior. In all cases with a rotated stiffener, the force coupling is constant in the prebuckling load range

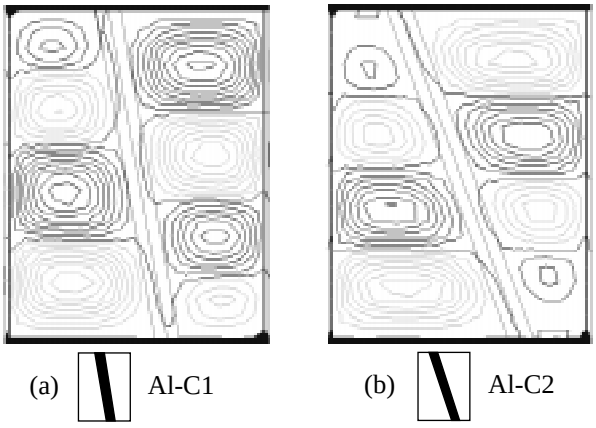

Fig. 8 Postbuckling shapes of all-aluminum panels with more-rigid stiffener rotated 10° and 20°.

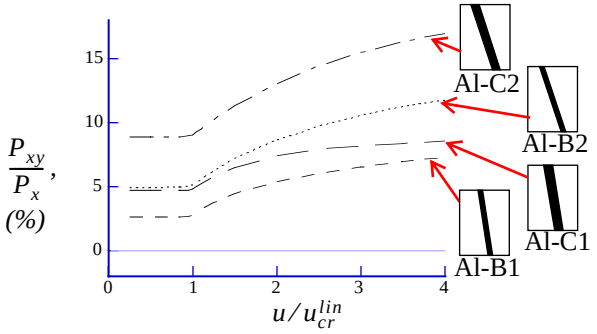

Fig. 9 Force-coupling response of all-aluminum panels with original and more-rigid stiffener.

and increases nonlinearly in the postbuckling load range. This increase in the force-coupling response in the postbuckling load range was also observed in the experiments for the composite panels with the rotated stiffeners reported in Ref. 5. The contour plots of the out-of-plane deformation indicate that the deformations in the skin-stiffener attachment region are small, and that rotating the stiffener causes the deformations in the postbuckled skin to be skewed, particularly in the regions of the skin that are directly adjacent to the stiffener. Since the deformations of the stiffener are small, the stiffener contribution to the response is expected to be linear over the entire range of loading. It is postulated that the increase in force-coupling response is related to the nonlinear response and skewed deformations of the postbuckled skin. To assess independently the effect of the skewed deformation state in the skin on the axial-shear coupling response, two cases are considered in which the rotated stiffeners are eliminated, and the out-of-plane displacements are constrained in the skin along a line where the stiffener was. Panel Al-w2 is created by eliminating the stiffener from panel Al-B2, and setting the *w* displacement equal to zero for the nodes in the skin that were originally under the stiffener web. Constraining the *w* displacement along a line simulates the out-of-plane support that a stiffener with a somewhat flexible cross section might provide. Panel Al-wdw2 is created to be similar to panel Al-w2, but the *w* displacement and the out-of-plane rotations, *Ru* and *Rv*, are constrained along the same line to simulate the support which a more-rigid stiffener would supply. Thus, these models simulate the out-of-plane support that a stiffener would supply, without including the inplane stiffness of the stiffener. Contour plots of the out-of-plane displacement in the skin at $u/u_{cr}^{lin} = 4$ are shown for panels Al-w2, and Al-wdw2 in Fig. 10. The contour plots shown in Figs. 10(a) and 10(b) closely resemble the contour plots for panels Al-B2 and Al-C2, shown in Figs. 6(c) and 8(b), respectively. The force-coupling versus end-shortening responses for panels Al-B2, Al-w2, and Al-wdw2 are compared in Fig. 11. The force-coupling responses for panels Al-w2 and Al-wdw2 are zero in the prebuckling load range, and increase to 4.71% and 6.07%, respectively, in the postbuckling load range. These results indicate similar increases in the force-coupling responses for panels Al-B2, Al-w2 and Al-wdw2, and support the postulate that the increase in the force-coupling response that is observed after skin buckling in panels with a rotated stiffener is due largely to the skewed deformations of the postbuckled skin.

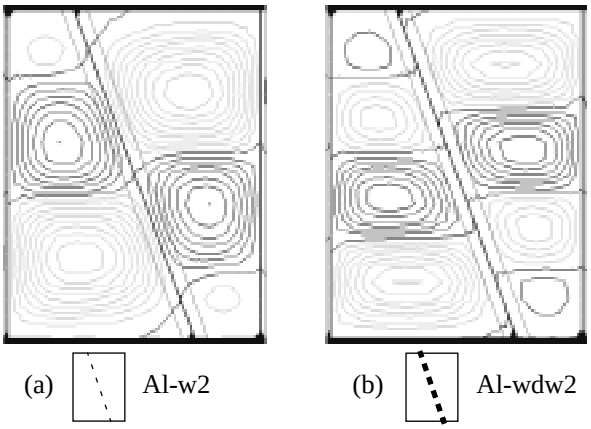

Fig. 10 Postbuckling shapes of all-aluminum panels with the rotated stiffener replaced with out-of-plane displacement constraints.

The issue of how skewness in the postbuckling deformation of the skin causes force coupling is now considered. In the unstiffened panels with displacement constraints considered above, the shear load P_{xy} is simply the integral of the shear stress resultant N_{xy} across the

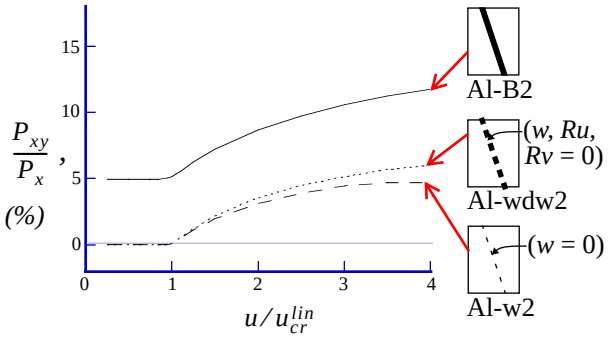

Fig. 11 Force-coupling responses of all-aluminum panel with original stiffener, and panels with the stiffener replaced with out-of-plane displacement constraints.

width of the panel. The panels are made of isotropic material, so A_{16} and A_{26} are zero, and the shear stress resultant N_{xy} is given by

$$N_{xy} = A_{66}\gamma_{xy}^{o} \quad , \tag{1}$$

where A_{ij} are the laminate membrane stiffnesses from classical lamination theory.[10] If P_{xy} is to be nonzero, then

$$\int \gamma_{xy}^{o} dy \neq 0 \quad . \tag{2}$$

If von Kármán nonlinear plate theory is applied,[10] then

$$\gamma_{xy}^{o} = \frac{\partial u_o}{\partial y} + \frac{\partial v_o}{\partial x} + \left(\frac{\partial w}{\partial x}\right)\left(\frac{\partial w}{\partial y}\right) \quad . \tag{3}$$

Skewness of the postbuckled shape affects the distribution of $(\partial w/\partial x)(\partial w/\partial y)$. For example, consider the contours of the skin out-of-plane displacements shown in Figs. 6(a) and 6(b). Enlarged views of the contour plots at the midlength of panels Al-B0 and Al-B1 are shown in Figs. 12(a) and 12(b), respectively. The deformation in panel Al-B0 is not skewed and $(\partial w/\partial x)(\partial w/\partial y) = 0$ across the entire width at the panel midlength. At cross sections above and below the midlength of panel Al-B0, $(\partial w/\partial x)(\partial w/\partial y)$ has nonzero values, but the integral of $(\partial w/\partial x)(\partial w/\partial y)$ across the width of the panel is equal to zero. The displacement contours for panel Al-B1 are skewed due to the support of the rotated stiffener. The quantity $(\partial w/\partial x)(\partial w/\partial y)$ at the panel midlength is approximately equal to zero on the left and right sides of the panel, but less than zero in the middle of the panel. This distribution of $(\partial w/\partial x)(\partial w/\partial y)$ creates a shear strain that does not integrate to zero, and thus, the panel shear load P_{xy} is nonzero.

The results presented in the previous paragraph have shown that rotating the stiffener can create a force-coupling response that is constant in the prebuckling load range, and increases nonlinearly in the postbuckling load range. While the results have shown that rotating the stiffener by a positive angle, i.e., $\alpha > 0$, creates positive

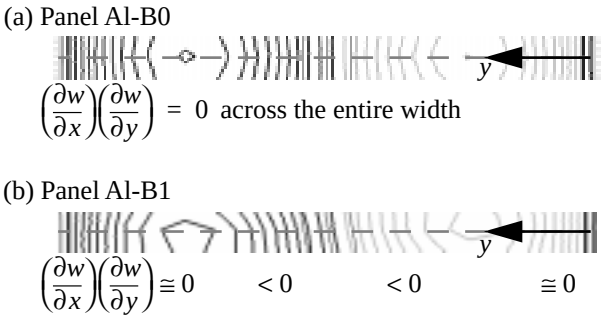

Fig. 12 Skewness in the out-of-plane displacements of the skin at panel midlength.

values of force coupling P_{xy}/P_x, it follows that rotating the stiffener by a negative angle creates negative values of force coupling. In regards to the *nonlinear* increase in force coupling after skin buckling, it is informative to examine the behavior of the forces P_x and P_{xy} independently. For example, consider the force-coupling response for panel Al-B2 that was shown in Fig. 7. The individual force components, P_x and P_{xy}, versus end shortening responses for this panel are shown in Figs. 13(a) and 13(b), respectively. The forces and end shortening are normalized by the linear buckling parameters, $(P_x)_{cr}^{lin}$ and u_{cr}^{lin}, respectively. The axial force versus end-shortening response shown in Fig. 13(a) displays a reduction in slope at the buckling load, indicating a reduction in axial stiffness that is typical of buckled stiffened panels. The response curve is nearly bilinear, with additional reductions in stiffness as the loading increases. When $u = 4.0\ u_{cr}$ the panel's axial stiffness is approximately 50% of its prebuckling axial stiffness. The shear force versus end-shortening response shown in Fig. 13(b) displays an increase in slope at the buckling load, and the response curve appears to be exactly bilinear. The force-coupling response that has been used throughout this study was defined on page 2 of this paper as the ratio of the shear force to the axial force. This definition provides a secant-type measure of the response at a given value of end shortening, but does not directly indicate the incremental (tangent) local behavior of the response. The secant force-coupling response P_{xy}/P_x, and the tangent force-coupling response $\Delta P_{xy}/\Delta P_x$, are computed for panel Al-B2 and compared in Fig. 13(c). Structural designers may be more interested in the tangent force coupling if they are concerned with controlling the incremental response of a structure as it is subjected to incremental loads. As indicated in Fig. 13(c), the tangential force-coupling response can vary significantly when the skin buckles.

Effect of Skin Anisotropy

To examine the effect of the skin anisotropy on the axial-shear coupling response of the stiffened panels,

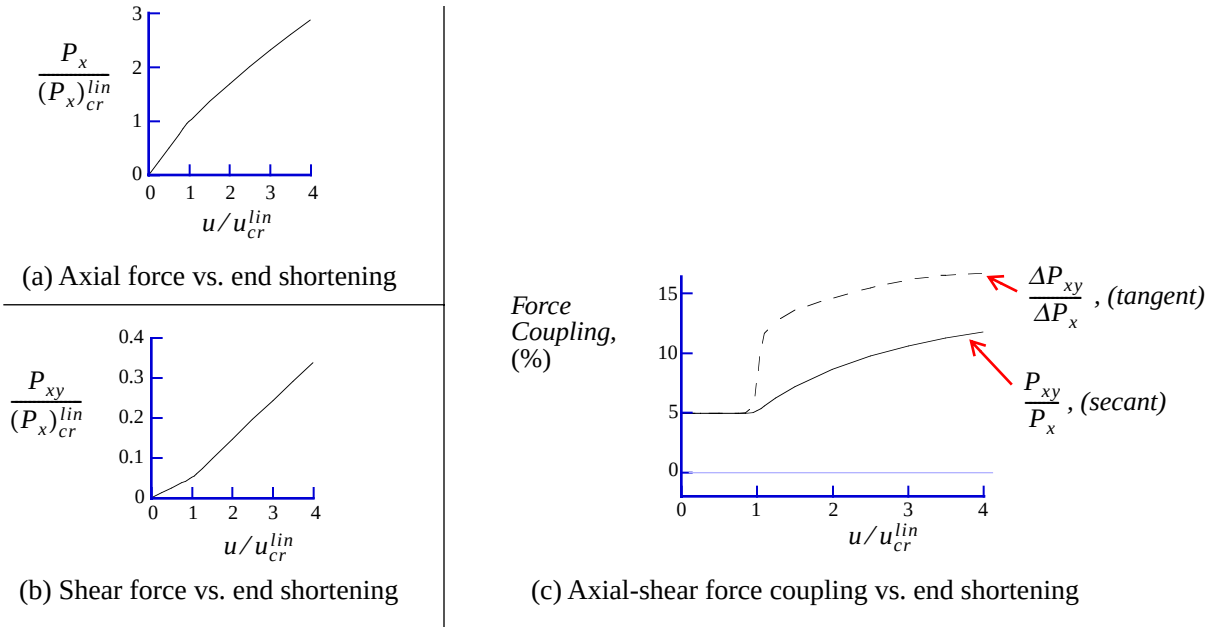

Fig. 13 Force coupling for panel Al-B2: individual force components and secant versus tangent force coupling.

panel configurations are considered which have an unrotated stiffener. The panels are assumed to be constructed entirely from Hercules, Inc. AS4-3502 graphite-epoxy unidirectional preimpregnated tape, with the material properties in Table 2 applied. The stiffener definition for these panels is the same as for the panels that were tested, i.e., a graphite-epoxy stiffener with $[\pm 45/0/90]_{2s}$ laminates and the cross section shown in Fig. 2.

For the panel configurations that were tested in Ref. 5, a nominal skin laminate construction was specified, and the entire laminate was rotated relative to the principal loading direction. Rotating a laminate typically modifies the membrane and bending stiffnesses. The skin constructions that are considered in the present study are not specified and then rotated, but rather are prescribed exactly to isolate specific membrane and bending stiffness coupling terms. A few parameters are useful to quantify the degree of anisotropy in a laminate. The amount of membrane stiffness coupling is reflected by the value of the equivalent membrane coefficient of mutual influence $\eta_{xy,x}^{o}$, defined as

$$\eta_{xy,x}^{o} = \frac{a_{16}}{a_{11}} \quad . \tag{4}$$

The amount of bending stiffness coupling is reflected by the value of the equivalent flexural coefficient of mutual influence $\eta_{xy,x}^{f}$, defined as

$$\eta_{xy,x}^{f} = \frac{d_{16}}{d_{11}} \quad , \tag{5}$$

and the values of the anisotropic parameters,

$$\gamma = \frac{D_{16}}{(D_{11}^3 D_{22})^{0.25}} \qquad \delta = \frac{D_{26}}{(D_{11} D_{22}^3)^{0.25}} \quad , \tag{6}$$

defined by Nemeth in Ref. 11. Results are subsequently presented for four different skin laminates. All of the skin laminates are 16-ply-thick symmetric laminates. The laminates have two 0° plies, two 90° plies, and the remaining twelve plies are a combination of -30° and 30° plies. The anisotropy of the laminates is altered by replacing -30° plies with 30°plies, and by changing the laminate stacking sequence. The stacking sequences for the selected laminates and values of the parameters which reflect their various degrees of anisotropy are listed in Table 2. The skin laminate 'c' has minimal anisotropy, and serves as a benchmark configuration. Laminate 'd' has a higher number of 30° plies to create membrane stiffness coupling, yet has a stacking sequence which minimizes the bending stiffness coupling. For laminate 'd', $\eta_{xy,x}^{o}$ is negative, indicating a negative membrane stiffness coupling. Laminate 'e' has zero membrane stiffness coupling, but has large negative bending stiffness coupling, as reflected in Table 2 by the negative value of $\eta_{xy,x}^{f}$. Laminate 'f' includes both negative membrane and negative bending stiffness coupling.

The panels, identified as B0c, B0d, B0e, and B0f, designate panel configurations with the unrotated stiffener, and skin laminates 'c', 'd', 'e', and 'f', respectively. The prebuckling stiffnesses for these panels are 17,250; 16,290; 17,250; and 16,290 kips, respectively. The linear buckling loads are 7.04, 6.37, 6.02, and 5.69 kips, respectively. Thus, the reductions in buckling load

Table 2 Laminates with Various Types of Anisotropy

Skin ID.	Lay-up	$\eta^{o}_{xy,\,x}$	$\eta^{f}_{xy,\,x}$	γ	δ
c	$[\pm 30/90/\mp 30/0/\mp 30]_s$	0.00	-0.03	0.02	0.01
d	$[-30/90/30_2/0/30_3]_s$	-0.76	0.03	0.01	0.01
e	$[30_3/90/0/-30_3]_s$	0.00	-1.06	0.45	0.25
f	$[30_3/90/30_2/0/-30]_s$	-0.76	-1.30	0.56	0.31

due to skin membrane stiffness coupling, bending stiffness coupling, and combined membrane and bending stiffness coupling, are 9%, 14%, and 19%, respectively, relative to the benchmark panel with minimal anisotropy. The reductions in the buckling load that occur when the skin laminate is highly anisotropic are consistent with the findings reported in Refs. 11 and 12. Contour plots of the out-of-plane displacement in the skin at $u/u_{cr}^{lin} = 4$ are shown in Fig. 14. Panel B0c has the most symmetric deformation shape. The membrane stiffness coupling in panel B0d causes the skin to buckle under combined compression and shear. The shear load causes slight skewing of the deformation pattern for panel B0d. Bending stiffness coupling in panels B0e and B0f causes the skin deformations to have substantial skewing, but in the opposite direction of the skewing shown for panel B0d.

The force-coupling versus end-shortening responses for these panels are shown in Fig. 15. The force coupling for panel B0c is approximately zero, as expected. The negative membrane stiffness coupling in panel B0d produces a force-coupling response that is 12.00% in the prebuckling load range, and decreases to 6.05% in the postbuckling load range. The negative bending stiffness coupling in panel B0e does not produce any force coupling until the skin buckles, and then the force coupling increases to 2.88% in the postbuckling load range. Panel B0f has the same membrane stiffness coupling as panel B0d, and thus has an equal amount of force coupling in the prebuckling response. The force-coupling response of panel B0f reduces after the skin buckles, but the negative bending stiffness coupling causes the reduction in force coupling to be less for panel B0f than it was for panel B0d. The force-coupling response for panel B0f ranges from 12.01% to 9.50%, and resembles the sum of the responses for panels B0d and B0e.

The axial-shear coupling response for panel B0f described above is very significant. This panel has negative membrane stiffness coupling and negative bending stiffness coupling, each of which creates a positive contribution to the force-coupling response. Negative membrane stiffness coupling becomes less effective in creating force coupling, i.e., the force-coupling response decreases, after the skin buckles. In contrast, negative

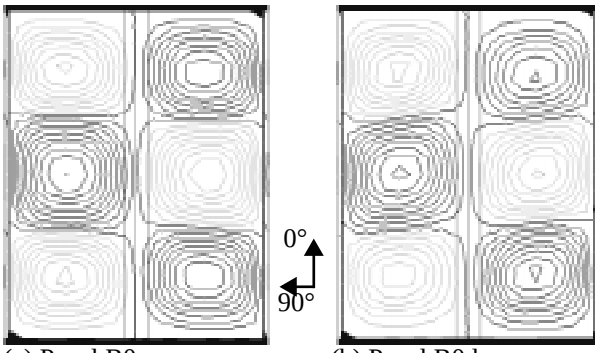

(a) Panel B0c, $[\pm 30/90/\mp 30/0/\mp 30]_s$

(b) Panel B0d, $[-30/90/30_2/0/30_3]_s$

(c) Panel B0e, $[30_3/90/0/-30_3]_s$

(d) Panel B0f, $[30_3/90/30_2/0/-30]_s$

Fig. 14 Postbuckling shapes of panels with the unrotated stiffener and anisotropic skins.

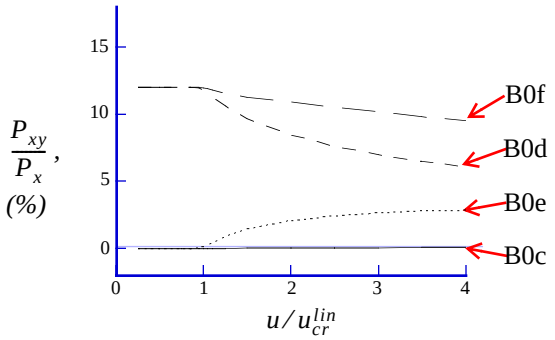

Fig. 15 Force-coupling response of panels with the unrotated stiffener and anisotropic skins.

bending stiffness coupling becomes more effective in creating force coupling, i.e., the force-coupling response increases, after the skin buckles. By applying both mechanisms, negative membrane stiffness coupling and negative bending stiffness coupling, in the same panel, the loss in effectiveness of one mechanism is offset in part by the increase in effectiveness of the second mechanism, and the net effect is that the force-coupling response is more uniform over the entire range of loading. The membrane and bending stiffness terms, as defined in Ref. 10, can be tailored somewhat independently. The membrane stiffness terms A_{ij}, represent a simple summation of lamina properties that is independent of the z-location of each lamina. In contrast, the bending stiffness terms D_{ij} are defined such that the contribution of each lamina to D_{ij} is weighted by the square of the z-location of the lamina. Therefore, it is possible to prescribe the percentage of lamina in specific orientations to tailor the A_{ij} terms, and then adjust the z-locations of the lamina by specifying the stacking sequence to tailor the D_{ij} terms. In panel B0f, the number of 30°plies is greater than the number of -30° plies to provide negative membrane stiffness coupling, and the -30° plies are located at the midplane of the laminate, while the 30° plies a located closer to the upper and lower surface of the laminate, to provide negative bending stiffness coupling.

Variations in Force-coupling Response in the Postbuckling Load Range for Panels with Skin Anisotropy

In the results shown in the previous paragraph, negative bending stiffness coupling was responsible for increases in force coupling after skin buckling. Bending stiffness coupling causes skewing of the skin deformations, as was shown in Fig. 14(c), and when presenting the results for rotated stiffeners previously, it was explained how skewing of the skin deformations can increase the force-coupling response in the postbuckling load range. In contrast, results have shown that negative membrane stiffness coupling in the skin creates a force-coupling response that is uniform in the prebuckling load range and reduces nonlinearly after skin buckling. To explain this behavior, additional details of the force-coupling response for panel B0d are shown in Fig. 16. The individual force components, P_x and P_{xy}, versus end-shortening responses for panel B0d are shown in Figs. 16(a) and 16(b), respectively. The axial force versus end-shortening response shown in Fig. 16(a) displays the typical reduction in slope at the buckling load. The response curve is nearly bilinear, with additional reductions in stiffness occurring as the load increases. The shear force versus end shortening response shown in Fig. 16(b) displays a sharp decrease in slope at the buckling load. This decrease in slope strongly contrasts with the increase in slope of the shear force response for the panel with a rotated stiffener, shown in Fig. 13(b). The secant force-coupling response, P_{xy}/P_x, and tangent force-coupling response, $\Delta P_{xy}/\Delta P_x$, are compared in Fig. 16(c). The large reduction in the tangential force-coupling response after skin buckling occurs reflects the very low slope of the shear force response curve and represents a substantial change in the behavior of the incremental response of the panel. The reduction in shear stiffness reported above resembles the results presented by Stein[13] on the postbuckling response of unstiffened plates in combined compression and shear. Stein observed that plates buckled in compression can display very large reductions in shear stiffness.

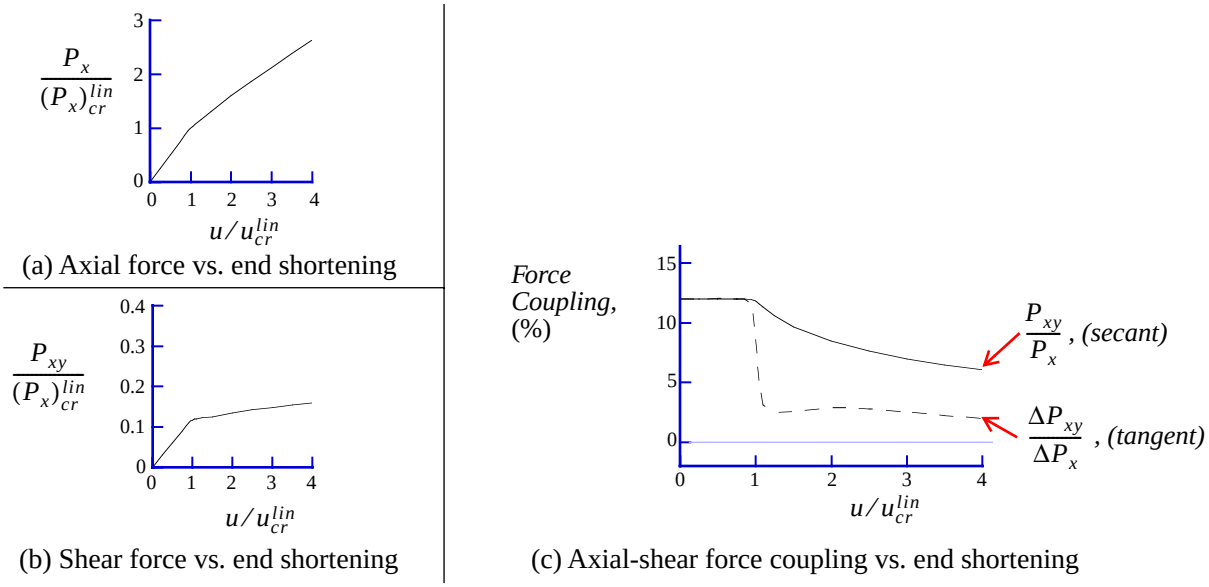

Fig. 16 Force coupling for panel B0d: individual force components and secant versus tangent force coupling.

The results presented in the previous paragraph have shown that anisotropy in the skin laminate creates a force-coupling response that is constant in the prebuckling load range. After the skin buckles, the force coupling due to negative membrane stiffness coupling decreases, while the force coupling due to negative bending stiffness coupling increases. While laminates were considered which created positive values of force coupling P_{xy}/P_x, changing the sign of the fiber orientations of these laminates would reverse the membrane and bending stiffness couplings and create negative values of force coupling.

Panel configurations have been considered which assess the effect of either skewed stiffeners or anisotropic skins on the force-coupling response. The results for these panels indicate that the amount of force coupling, and the behavior of the response in the postbuckling load range, is dependent upon which mechanism is employed to create stiffness coupling. Additional cases are subsequently considered which combine the mechanisms to tailor the axial-shear coupling response in the prebuckling and postbuckling load ranges.

Effects of Combining Skewed Stiffeners and Anisotropic Skins

Panel configurations which have the stiffener rotated 20° and have skin laminates with membrane and bending stiffness coupling are considered in this section. The original graphite-epoxy stiffener definition shown in Fig. 2 was used for these panels. Results are presented below for five skin laminates. Three of the laminates are laminates 'c', 'd', and 'e', which were defined in the preceding section. The stacking sequences for these laminates were shown previously in Table 2. Two additional laminates, designated as laminates 'dr' and 'er', are prescribed by changing the sign of the fiber orientations of laminates 'd' and 'e', respectively, to change the signs of the stiffness couplings of the laminates. Laminate 'dr' has a stacking sequence of $[30/90/-30_2/0/-30_3]_s$, and has large positive membrane stiffness coupling and minimal bending stiffness coupling. Laminate 'er' has a stacking sequence of $[-30_3/90/0/30_3]_s$, and has large positive bending stiffness coupling and minimal membrane stiffness coupling.

The panels, identified as B2c, B2d, B2dr, B2e, and B2er designate panel configurations with the stiffener rotated 20° and skin laminates 'c', 'd', 'dr', 'e', and 'er', respectively. Of these five panels, panel B2c is considered to be the benchmark configuration since skin 'c' has minimal anisotropy. The prebuckling stiffnesses for these panels are 16,880; 15,960; 15,860; 16,880; and 16,880 kips, respectively. The linear buckling loads are 5.44, 6.07, 4.45, 4.14, and 5.22 kips, respectively. Thus, when the stiffener is rotated, the panel with negative membrane stiffness coupling of the skin laminate has a linear buckling load that is 12% greater than, and the panel with positive membrane stiffness coupling has a linear buckling load that is 18% less than, the buckling load of the benchmark configuration with minimal anisotropy in the skin. The panels with skin laminates with negative and positive bending stiffness coupling show decreases in the buckling load of 24% and 4%, respectively. Contour plots of the out-of-plane displacement in the skin at $u/u_{cr}^{lin} = 4$ are shown in Fig. 17.

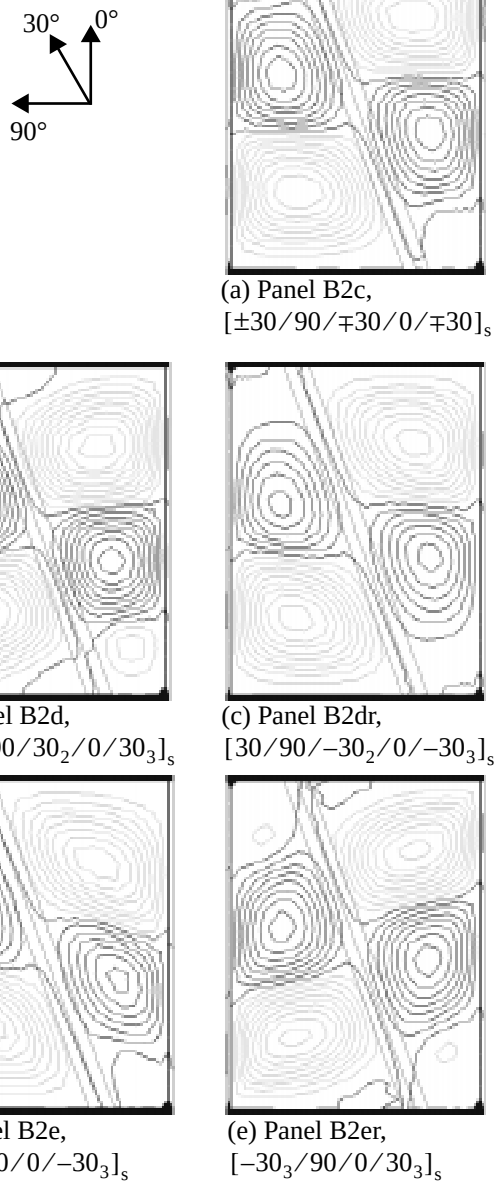

(a) Panel B2c, $[\pm 30/90/\mp 30/0/\mp 30]_s$

(b) Panel B2d, $[-30/90/30_2/0/30_3]_s$

(c) Panel B2dr, $[30/90/-30_2/0/-30_3]_s$

(d) Panel B2e, $[30_3/90/0/-30_3]_s$

(e) Panel B2er, $[-30_3/90/0/30_3]_s$

Fig. 17 Postbuckling shapes of panels with the stiffener rotated 20° and anisotropic skins.

The force-coupling versus end-shortening responses for these panels are shown in Fig. 18. The force-coupling responses for the panels that combine a rotated stiffener and anisotropic skin are shown in separate plots so that they can be compared to the force-coupling responses that are obtained when the rotated stiffener and anisotropic skins were applied separately. For example, the force-coupling response for panel B2d is compared to the force-coupling responses for panels B2c and B0d in Fig. 18(a). Panel B2c, which has the stiffener rotated 20° and negligible anisotropy, has a force-coupling response that is 4.81% in the prebuckling load range, and increases to 12.29% in the postbuckling load range. Panel B0d, considered in the previous section, has an unrotated stiffener and negative membrane stiffness coupling, and has a force-coupling response that is 12.00% in the prebuckling load range, but decreases to 6.05% in the postbuckling load range. When the rotated stiffener and negative membrane stiffness coupling are combined in panel B2d, it appears as if the responses of panels B2c and B0d are superimposed. The prebuckling responses add to give a larger response, and the increasing and decreasing responses after buckling partially offset each other. The net affect is that panel B2d has a large force-coupling response that varies by a small amount over the entire load range. The force-coupling response for panel B2d is 17.48% before buckling, and increases to 19.42% in the postbuckling load range.

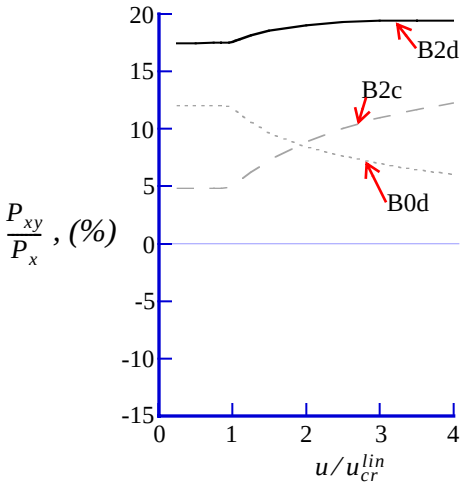

(a) Rotated stiffener and negative membrane stiffness coupling

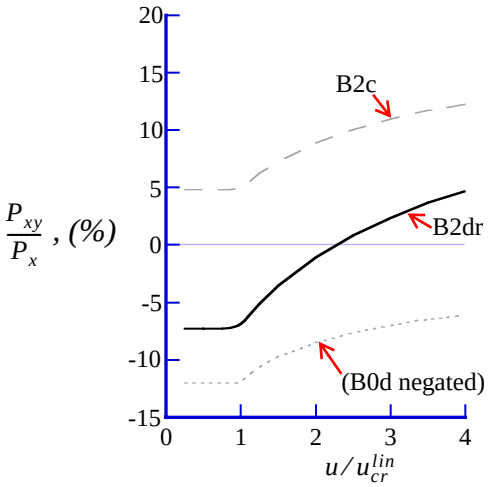

(b) Rotated stiffener and positive membrane stiffness coupling

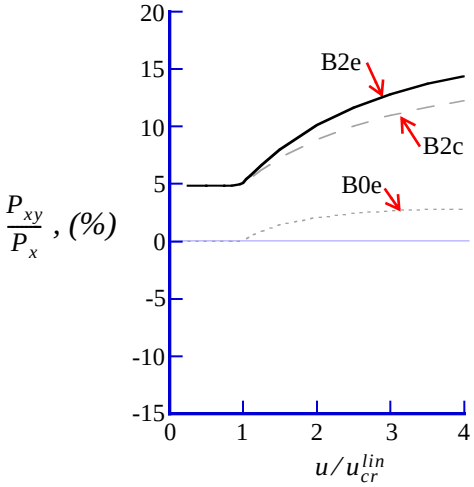

(c) Rotated stiffener and negative bending stiffness coupling

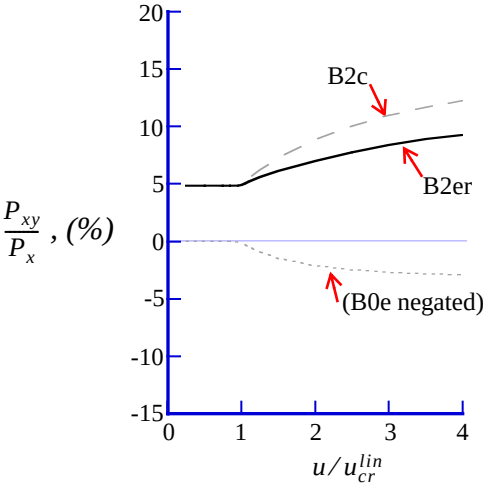

(d) Rotated stiffener and positive bending stiffness coupling

Fig. 18 Force-coupling response of panels which combine a rotated stiffener and anisotropic skins.

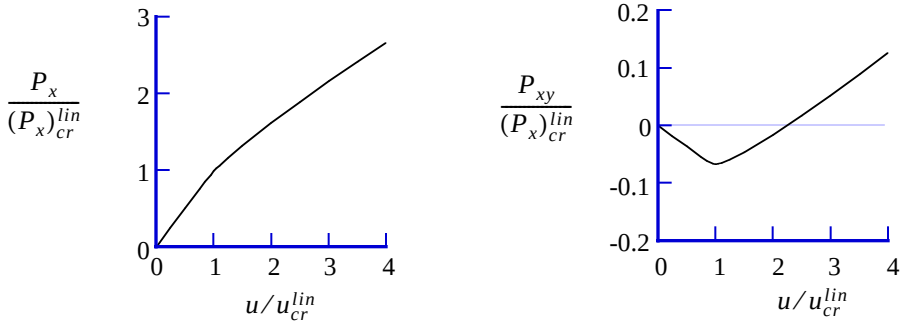

(a) Axial force vs. end shortening (b) Shear force vs. end shortening

Fig. 19 Individual force components for panel B2d.

The results for the case which combines a rotated stiffener with a skin laminate with positive membrane stiffness coupling are presented in Fig. 18(b). If an analysis were conducted with an unrotated stiffener and skin laminate 'dr', then the force-coupling response would be equal to the 'B0d negated' response shown in Fig. 18(b). The 'B0d negated' response is negative before buckling, and becomes less negative, i.e., increases, after skin buckling. When the rotated stiffener and positive membrane stiffness coupling are combined in panel B2dr, it appears as if the responses of panels B2c and 'B0d negated' are superimposed. The prebuckling responses partially offset each other, and the increasing responses after buckling are additive. The net effect is that panel B2dr has a force-coupling response that is -7.28% before buckling, and increases to 4.74% in the postbuckling load range. The individual force components, P_x and P_{xy}, versus end shortening responses for panel B2dr are shown in Figs. 19(a) and 19(b), respectively. The axial force versus end shortening response shown in Fig. 19(a) is typical of all of the panels. The shear force versus end shortening response shown in Fig. 19(b) is unique in that it has a negative slope during the initial loading and a positive slope after the skin buckles. The incremental shear force is positive immediately after the skin buckles, while the net shear force on the panel does not become positive until the load increases further into the postbuckling load range. The force-coupling response of panel B2dr, shown in Fig. 18(b), becomes positive when the shear force P_{xy} becomes positive.

The results for the case which combines a rotated stiffener with a skin laminate with negative bending stiffness coupling are presented in Fig. 18(c). Panel B0e, considered in the previous section, has an unrotated stiffener and negative bending stiffness coupling, and has a force-coupling response that is equal to zero in the prebuckling load range, but increases to 2.88% in the postbuckling load range. When the rotated stiffener and negative bending stiffness coupling are combined in panel B2e, it appears as if the responses of panels B2c and B0e are superimposed. Comparing the results for panels B2c and B2e shows that the negative bending stiffness coupling in panel B2e does not affect the force-coupling response before buckling occurs, but it does increase the force-coupling response in the postbuckling load range. The force-coupling response for panel B2e is 4.81% before buckling, and increases to 14.40% in the postbuckling load range.

The results for the case which combines a rotated stiffener with a skin laminate with positive bending stiffness coupling are presented in Fig. 18(d). If an analysis were conducted with an unrotated stiffener and skin laminate 'er', then the force-coupling response would be equal to the 'B0e negated' response shown in Fig. 2(d). When the rotated stiffener and positive membrane stiffness coupling are combined in panel B2er, the positive bending stiffness coupling does not affect the force-coupling response before buckling occurs, but it does reduce the amount of increase in the force-coupling response in the postbuckling load range. The force-coupling response for panel B2er is 4.81% before buckling, and increases to 9.30% in the postbuckling load range.

Summary of Cases Considered

The panel description, prebuckling stiffness, *EA*, the linear buckling parameters, $(P_x)_{cr}^{lin}$ and u_{cr}^{lin}, and the force-coupling response, (P_{xy}/P_x), in the prebuckling and postbuckling load ranges, are summarized in Table 3 for each stiffened panel configuration that was considered in the current study. The force-coupling response in the postbuckling load range is defined as (P_{xy}/P_x) at $u = 4.0\ u_{cr}$. In Table 3, the panels are listed by their panel identification code, or 'I.D.' The stiffener cross section of each panel is identified by code. Cross sections

Table 3 Summary of Parametric Study

I.D.	Stiffener		Skin Laminate	*EA* (kip)	Linear Buckling		P_{xy}/P_x, (%)	
	Cross Section	α (deg)			$(P_x)_{cr}^{lin}$ (kip)	u_{cr}^{lin} (mil)	Pre-buckle	Post-buckle
Al-B0	Al-B	0	Al-2024, t = 0.0771 in.	16,630	8.25	11.90	0.000	0.000
Al-B1	Al-B	10	Al-2024, t = 0.0771 in.	16,530	7.70	11.17	2.63	7.33
Al-B2	Al-B	20	Al-2024, t = 0.0771 in.	16,270	6.48	9.56	4.95	11.77
Al-C1	Al-C	10	Al-2024, t = 0.0771 in.	19,430	9.88	12.21	4.71	8.57
Al-C2	Al-C	20	Al-2024, t = 0.0771 in.	18,820	8.15	10.39	8.90	17.00
B0,0	B	0	$[\pm 45/\mp 45/0_3/90]_s$	16,650	7.71	11.12	0.000	0.080
B0,2	B	0	$[65/-25_2/65/20_3/-70]_s$	15,950	6.95	10.46	2.54	1.69
B2,0	B	20	$[\pm 45/\mp 45/0_3/90]_s$	16,270	5.72	8.44	4.97	12.15
B2,2	B	20	$[65/-25_2/65/20_3/-70]_s$	15,580	5.62	8.66	7.84	14.17
B2,n2	B	20	$[25/-65_2/25/-20_3/70]_s$	15,550	5.22	8.06	2.57	10.24
B0c	B	0	$[\pm 30/90/\mp 30/0/\mp 30]_s$	17,250	7.04	9.79	0.000	0.080
B0d	B	0	$[-30/90/30_2/0/30_3]_s$	16,290	6.37	9.38	12.00	6.05
B0e	B	0	$[30_3/90/0/-30_3]_s$	17,250	6.02	8.37	0.000	2.88
B0f	B	0	$[30_3/90/30_2/0/-30]_s$	16,300	5.69	8.38	12.00	9.50
B2c	B	0	$[\pm 30/90/\mp 30/0/\mp 30]_s$	16,880	5.44	7.73	4.81	12.29
B2d	B	20	$[-30/90/30_2/0/30_3]_s$	15,960	6.07	9.13	17.48	19.42
B2dr	B	20	$[30/90/-30_2/0/-30_3]_s$	15,860	4.45	6.73	-7.28	4.74
B2e	B	20	$[30_3/90/0/-30_3]_s$	16,880	4.14	5.89	4.81	14.40
B2er	B	20	$[-30_3/90/0/30_3]_s$	16,880	5.22	7.42	4.81	9.30

'Al-B' and 'Al-C' refer to the nominal and more-rigid aluminum stiffeners, respectively. Cross section 'B' refers to the nominal graphite-epoxy stiffener that was used for all of the composite panels. The all-aluminum panels are listed first in Table 3, followed by the composite panels that were tested, and then the additional composite panels that were discussed in the present paper.

Concluding Remarks

The results of a numerical parametric study of the potential for tailoring the prebuckling and postbuckling response of stiffened composite panels with axial-shear stiffness coupling have been presented. Specific configurations are considered which independently assess and characterize the effects of stiffener orientation, stiffener stiffness, skin membrane stiffness coupling, and skin bending stiffness coupling, on a stiffened panel's axial-shear coupling response. The results help identify different mechanisms for axial-shear coupling that produce a wide range of load-dependent structural responses. These results provide insight into the effects of tailoring the stiffener components as well as the skin anisotropy of stiffened composite panels to obtain unique structural responses that may not possible with metallic panels or with unstiffened composite panels.

References

[1]Starnes, J. H., Jr., Knight, N. F., Jr., and Rouse, M., “Postbuckling Behavior of Selected Flat Stiffened Graphite-Epoxy Panels Loaded in Compression,” *AIAA Journal*, Vol. 23, No. 8, August 1985, pp. 1236-1246.

[2]Dickson, J. N., Biggers, S. B., and Starnes, J. H., Jr., “Stiffener Attachment Concepts for Graphite-Epoxy Panels Designed for Postbuckling Strength,” AFWAL-TR-85-3094, June 1985, pp. v(a)95-v(a)109.

[3]Gimmestad, D., “An Aeroelastic Optimization Procedure for Composite High Aspect Ratio Wings,” AIAA Paper No. 79-0726, April 1979.

[4]Mansfield. E. H., “Some Structural Parameters for Aero-Isoclinic Wings,” *Aircraft Engineering*, Vol. 24, No. 283, September 1952, pp. 263-264.

[5]Young, R. D., Starnes, J. H., Jr. and Hyer, M. W., “Effects of Skewed Stiffeners and Anisotropic Skins on the Response of Compression-Loaded Composite Panels,” Proceedings of the Tenth DoD/NASA/FAA Conference of Fibrous Composites in Structural Design, Hilton Head Island, SC, November 1-4, 1993, Naval Air Warfare Center Report No. NAWACADWAR-94096060, Vol. 1, April 1994, pp. II-109 to II-123.

[6]Young, R. D., Starnes, J. H., Jr., and Hyer, M. W., “Accurate Modeling of the Postbuckling Response of Composite Panels with Skewed Stiffeners,” AIAA Paper No. 97-1306, April 1997.

[7]Young, R. D., “Prebuckling and Postbuckling Behavior of Stiffened Composite Panels with Axial-shear Stiffness Coupling”, Ph.D. thesis, Department of Engineering Science and Mechanics, Virginia Polytechnic Institute and State University, Blacksburg, VA, 1996.

[8]Rankin, C. C., Brogan, F. A., W. A. Loden, and Cabiness, H. D., "STAGS User Manual, Version 3.0," Lockheed Martin Missiles & Space Co., Inc., Rept. LMSC P032594, March 1999.

[9]Rankin, C. C., and Brogan, F. A., "The Computational Structural Mechanics Testbed Structural Element Processor ES5: STAGS Shell Element," NASA Contractor Report 4358, May 1991.

[10]Chia, C. Y., *Nonlinear Analysis of Plates*, McGraw-Hill, New York, 1980.

[11]Nemeth, M. P., “Importance of Anisotropy on Buckling of Compression-Loaded Symmetric Composite Plates,” *AIAA Journal*, Vol. 24, No. 11, November 1986, pp. 1831-1835.

[12]Jensen, D. W., and Lagace, P. A., “Influence of Mechanical Couplings On the Buckling and Postbuckling Behavior of Anisotropic Plates,” AIAA Paper No. 86-0880, May 1986.

[13]Stein, M., “Postbuckling of Long Orthotropic Plates in Combined Shear and Compression,” AIAA Paper No. 83-0876, May 1983.